Chemistry–A European Journal
Research Article
doi.org/10.1002/chem.202302779
Chemistry Europe
European Chemical Societies Publishing
www.chemeurj.org

Hot Paper

Special Collection

Fluorinated Benzimidazole-Linked Highly Conjugated Polymer Enabling Covalent Polysulfide Anchoring for Stable Sulfur Batteries

Sattwick Haldar,*[a] Arafat H. Khan,[b] Ankita De,[a] Fanny Reichmayr,[c] Ahiud Morag,[d, e] Minghao Yu,[d] Andreas Schneemann,[a] and Stefan Kaskel*[a, f]

Sulfur is one of the most abundant and economical elements in the p-block family and highly redox active, potentially utilizable as a charge-storing electrode with high theoretical capacities. However, its inherent good solubility in many electrolytes inhibits its accessibility as an electrode material in typical metal-sulfur batteries. In this work, the synthetically designed fluorinated porous polymer, when treated with elemental sulfur through a well-known nucleophilic aromatic substitution mechanism (S_NAr), allows for the covalent integration of polysulfides into a highly conjugated benzimidazole polymer by replacing the fluorine atoms. Chemically robust benzimidazole linkages allow such harsh post-synthetic treatment and facilitate the electronic activation of the anchored polysulfides for redox reactions under applied potential. The electrode amalgamated with sulfurized polymer mitigates the so-called polysulfide shuttle effect in the lithium-sulfur (Li–S) battery and also enables a reversible, more environmentally friendly, and more economical aluminum-sulfur (Al–S) battery that is configured with mostly p-block elements as cathode, anode, and electrolytes. The improved cycling stabilities and reduction of the overpotential in both cases pave the way for future sustainable energy storage solutions.

Introduction

The pursuit of sustainable and cost-effective energy storage solutions has become an urgent global endeavor due to mounting environmental concerns[1] and increasing energy demands.[2] In this quest, p-block elements found in groups 13 to 18 of the periodic table have emerged as promising candidates, owing to their abundance and profound redox activity for energy storage.[3] For instance, Group 14 and 15 elements graphite (C),[4] silicon (Si),[5] germanium (Ge),[6] and phosphorus (P)[7] have been studied for their high capacity as anodes in metal-ion batteries. However, they face challenges such as volume expansion during cycling and low energy densities. Meanwhile, Group 16 and 17 elements consisting of chalcogens (sulfur, selenium, and tellurium)[8] and certain halogens (fluorine, chlorine, bromine, and iodine)[9] are also considered high-energy cathode materials for various rechargeable batteries. Among these elements, sulfur, particularly octasulfur, stands out as one of the most abundant and cost-efficient sources of cathode materials

within the p-block family.[10] It offers high theoretical capacities with multivariate redox properties and multistep redox activity as a charge-storing electrode.[11] Sulfur's two lone pair electrons can easily bind with metal ions, and its accessible d-orbital stabilizes the intermediates formed during redox reactions in the presence of metal ions. Despite these advantages, practical application in metal-sulfur batteries has been hindered by inherent dissolution issues of sulfur in electrolytes, limiting its viability as an electrode material in conventional battery setups.[12]

By encapsulating sulfur in porous supports like porous carbon,[13] porous polymer,[14] the high-surface-area containing

[a] Dr. S. Haldar, A. De, Dr. A. Schneemann, Prof. Dr. S. Kaskel
Chair of Inorganic Chemistry I
Technische Universität Dresden
01069 Dresden (Germany)
E-mail: sattwick.haldar@tu-dresden.de
stefan.kaskel@tu-dresden.de
[b] Dr. A. H. Khan
Chair of Bioanalytical Chemistry
Technische Universität Dresden
01069 Dresden (Germany)
[c] F. Reichmayr
Chair of Electrochemistry
Technische Universität Dresden
01069 Dresden (Germany)
[d] Dr. A. Morag, Dr. M. Yu
Center for Advancing Electronics Dresden (cfaed) and Faculty of Chemistry and Food Chemistry
Technische Universität Dresden
01069 Dresden (Germany)
[e] Dr. A. Morag
Max Planck Institute of Microstructure Physics
Weinberg 2, 06120 Halle (Germany)
[f] Prof. Dr. S. Kaskel
Fraunhofer Institute for Material and Beam Technology (IWS)
Winterbergstraße 28, 01277, Dresden (Germany)

Supporting information for this article is available on the WWW under https://doi.org/10.1002/chem.202302779

Part of a Special Collection on the p-block elements.

metal-organic frameworks (MOFs),[15] or covalent-organic frameworks (COFs) with polar functionalities,[16,17] the problems of dissolution in the electrolyte can be addressed. Nonetheless, this approach lacks the covalent connection to the porous host, leading to a lack of electronic activation of active sulfur materials and providing lower capacity than theoretically expected. Thus, a direct covalent connection of the sulfur entities to the conjugated polymeric support would be beneficial, reducing the polysulfide shuttle effect and providing an electronic connection.[18] In this context, COFs with halo substitutions are already promising materials but challenges lie in bulk scale-up synthesis with good purities because it requires a complicated template-mediated procedure.[19]

Sometimes, these COFs undergo destruction during the harsh post-synthetic sulfurization. However, the template-free electronically conjugating polymers could be an alternate solution for large-scale production with great purities.[20]

This work focuses on designing and synthesizing a conjugated benzimidazole-linked porous polymer with fluorine substitution, specifically tailored for the covalent integration of polysulfides. This synthetic strategy leverages the well-known S_NAr mechanism[21] that mainly occurs with the aromatic substitution of electronegative halo atoms from the aromatic rings, i.e. replacement of fluorine atoms with polysulfides (Scheme 1).[22] The chemically more robust benzimidazole linkages[23] compared to other covalent linkages such as imine, polyimide, and boronate ester allow for this harsh post-synthetic modification without breaking the framework skeleton.[24] As a result, this integration effectively mitigates the "polysulfide shuttle effect", commonly observed in sulfur electrodes. Through detailed experimentation and characterization, this sulfurized polymer demonstrates the capability to serve as a highly reversible and efficient electrode material in Li–S batteries with long-cycle stability.

Furthermore, along with the standard Li–S battery, it enables the development of an Al–S battery configuration, considering that aluminum minerals are more abundant than lithium, making it a more sustainable and cost-effective option with multi-electron transfer for high volumetric capacity.[25,26] Remarkably, this novel battery system relies mostly on easily biodegradable p-block elements, while constructing the cathode, anode, and electrolytes, contributing to its environmental friendliness.

The outcomes of this research showcase improved cycling stabilities and a reduction in overpotential for both Li–S and Al–S battery configurations. This opens the doors for a promising future of sustainable energy storage solutions, with the full-fledged utility of the p-block elements.

Results and Discussion

Synthesis and characterization of fluorine-substituted benzimidazole-linked polymer (DUT-178)

Orthodiamine reacts with aldehydes, undergoing ring cyclization reactions, resulting in the formation of an aromatic benzimidazole compound.[27] Using this strategy, a C_3 symmetric triphenylene-2,3,6,7,10,11-hexaamine (HATP)[28] was reacted with a C_2 symmetric 2,3,5,6-tetrafluoroterephthalaldehyde (TFTP) to configure a benzimidazole-linked conjugated polymer with ample fluorine substitution (Figure 1A, Scheme S1). The template-free synthesis procedure involves two steps. Firstly, homogeneous mixing of HATP and TFTP in N,N-Dimethylformamide (DMF) at −40 °C for 6 hours, followed by raising the temperature to 130 °C under O_2 bubbling. The resulting product yielded a brownish-yellow powder after vigorous soxhlet extraction in tetrahydrofuran (THF), followed by supercritical CO_2 drying. The use of the supercritical CO_2 drying method enhanced the porosity of the polymer by removing trace amounts of high-boiling DMF solvent and trapped water from the framework, as evidenced by the comparative physisorption analysis (Figure S1) with the Soxhlet-extracted sample. The formation of the benzimidazole linkage is irreversible compared to the imine bond, making the formation of crystalline materials[29,30] very difficult and yielding very little, resulting in low microporosity (Scheme S1, Figure S2). Since bulk sulfurization requires a good yield of materials with great purity from each batch of synthesis and reasonable microporosity for the diffusion of molten sulfur, we chose the path of easily scalable polymer synthesis, instead of preparing a crystalline benzimidazole linked COF.

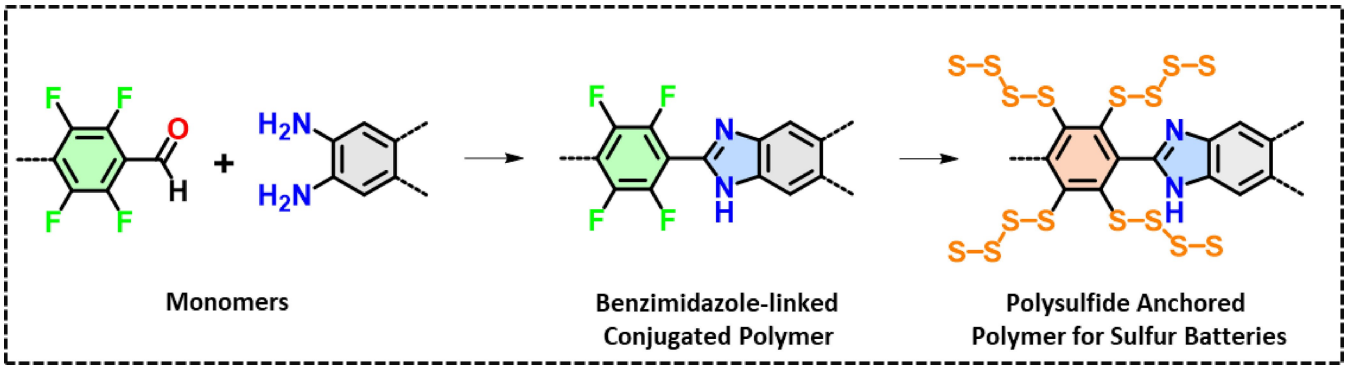

Scheme 1. Designer sulfur-anchored polymer synthesis for metal-sulfur batteries.

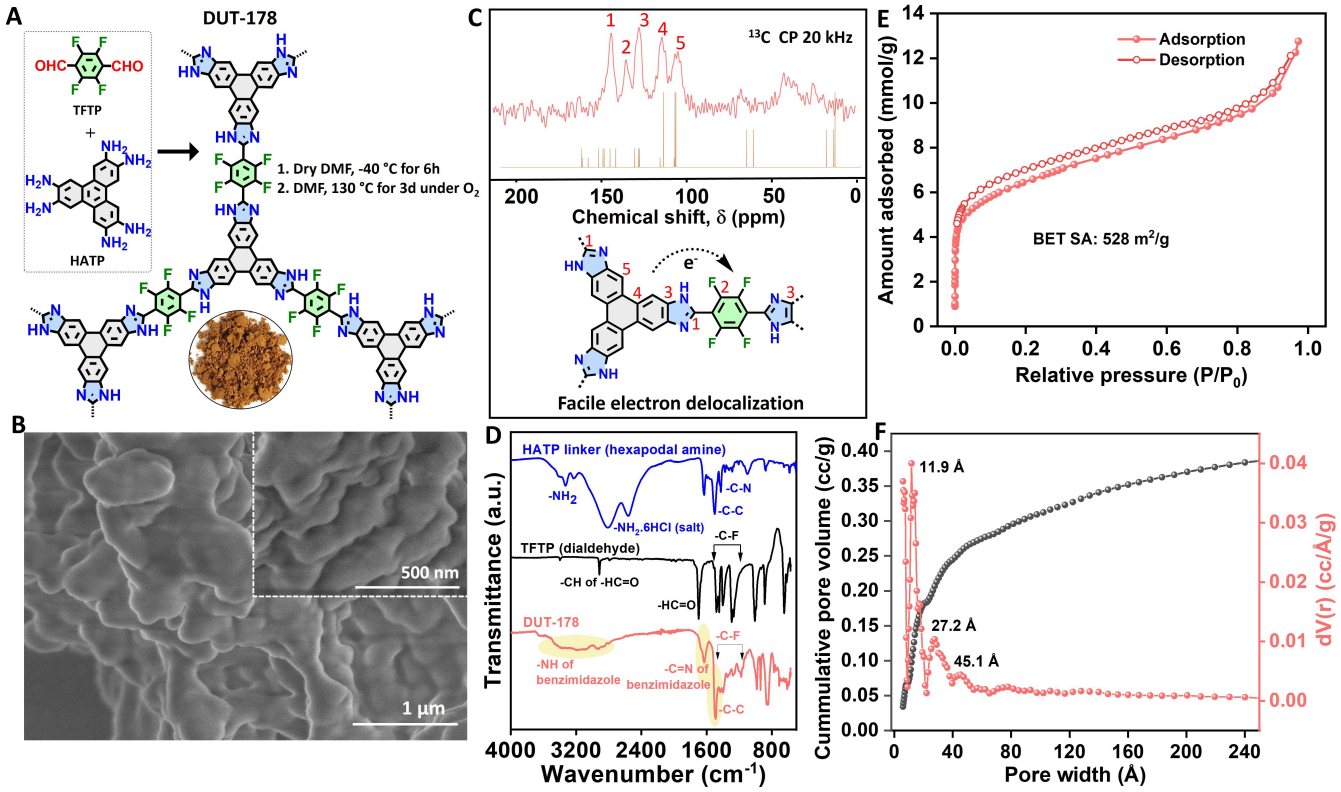

Figure 1. A. Synthetic route toward DUT-178 from its monomer. **B**. FE-SEM images of the DUT-178. An inset image showed an amalgamation of flakes of the polymer. **C**. ^{13}C CP MAS NMR spectrum of DUT-178 and the comparison with the model unit's predicted chemical shifts. **D**. FT-IR spectra of DUT-178 and the comparison with its building monomers. **E**. N_2 physisorption isotherm of DUT-178 recorded at 77 K. **F**. Pore width and cumulative pore volume distribution obtained through the NLDFT method from the adsorption branch of N_2 isotherm at 77 K.

Plausible electron delocalization occurring from electron-rich HATP to electron-deficient TFTP units within the polymer, their π-aromatic clouds, and the robust aromatic benzimidazole linkage, maintained the overall planarity of the structure (Scheme S2). The resulting high electronic conjugation and planarity of all aromatic constituents created a rigid, and flaky morphology, as observed in field emission scanning electron microscopy (FE-SEM) studies (Figure 1B, Figure S3). These planar flakes easily amalgamate into layers, even though it's not originally a layered structure. This polymer and all its functional groups were thoroughly characterized by ^{13}C Cross-Polarization magic angle spinning nuclear magnetic resonance (^{13}C CP MAS NMR), ^{1}H depth MAS NMR, Fourier Transform Infrared Spectroscopy (FT-IR), and Powder X-Ray Diffraction (PXRD) (Figures 1C–D, Figure S4–S5). A strong signal at 146 ppm in ^{13}C CP MAS NMR confirmed the formation of the aromatic benzimidazole ring (Figure 1C).[22,27] As the aromatic carbons and attached protons from the triphenylene and phenyl units are chemically very similar in the environment, clear distinguishing was not possible. However, matching the simulated ^{13}C CP MAS NMR pattern with the modeled structure confirms the formation of the expected polymeric structure.[31] The broad aromatic proton signals centered around 8.5 ppm in ^{1}H MAS NMR suggest the strong electron delocalization within the triphenylene rings and benzimidazole rings of the polymer (Figure S4). The presence of benzimidazole proton adjacent to the high electron withdrawing perfluorinated ring resulted in a higher chemical shift for the imidazole –NH around 12–13 ppm than expected. Distinguishing the –NH signals, including those from benzimidazole, in broad ^{1}H depth MAS NMR is challenging due to interference from adsorbed solvent, strong electron delocalization within the structure, and the absence of crystalline ordering.[32–33] Deconvolution of the ^{1}H NMR spectra of the DUT-178 polymer allowed differentiation of the benzimidazole's –NH signal (Figure S4C) The absence of IR stretching frequencies of the –NH_2 groups in HATP, and the –CH vibration from the –CHO groups in TFTP, confirmed the completeness of the ring cyclization. This is supported by the appearance of a stretching frequency at 1632 cm^{-1} and vibrational frequencies at 3230 cm^{-1} for the benzimidazole's –C=N and –NH groups, respectively (see Figure 1D). Indeed, the observation of many moderately strong –C–F stretching and vibrational frequencies ranging from 1170 cm^{-1} to 1420 cm^{-1} confirms the presence of perfluorinated phenyl rings of this polymer which originate from the TFTP linker. Additionally, the absence of any diffraction peaks originating from the linker in the powder diffraction pattern indicates the purity of the polymer (Figure S5). In this case, the planarity of fused aromatic rings from HATP acts as a self-template to obtain a moderate surface area of 528 m^2/g, as observed from the N_2 physisorption at 77 K (Figure 1 E). This adsorption measurement features a Type I profile, with a mixture of micropores of 12 Å diameter, as well as mesopores of 27 Å, and 45 Å, as estimated from the non-local density functional theory (NLDFT) fitting of the isotherm (Figure 1F).

Synthesis and characterization of sulfurized DUT-178 (S-DUT-178)

In the next step of covalent polysulfide anchoring, the porous nature of the synthesized polymer provided an advantage for the proper encapsulation of sulfur in its molten state at 150 °C within the polymer's pores. The porosity of the polymer facilitates the diffusion of highly reactive polysulfide species in its molten state, which were generated after opening the octasulfur ring at an elevated temperature of 350 °C. This leads to the substitution of most of the fluorine with polysulfide chains following the S_NAr reaction mechanism (Scheme S3, Figure 2A).[22] A comparison of the real intensity of ^{19}F MAS depth NMR[34] spectra before and after sulfurization indicated an almost 90% reduction in the number of fluorine atoms when measured on a similar mass of materials (Figure 2B). In this case, the ^{19}F signals at 125 ppm originating from the secondary reference of the terminating TFTP units of the polymers[35] assisted in calculating the mass loss of fluorine from the polymer which appeared as a broad signal centered around 148 ppm. Moreover, the resolution of the ^{13}C CP MAS NMR spectra became poor, and significant line broadening was observed, even after long contact time measurements, indicating a huge interference from sulfur entities (Figure S6). The appearance of a new signal in the ^{1}H MAS NMR spectrum near 1.5 ppm suggested the presence of terminal –SH proton from the covalently anchored sulfur chain.[36] The presence of benzimidazole protons at 12–13 ppm and the signal broadening of phenylic aromatic protons from 6–9 ppm confirmed the integrity of the benzimidazole network and strong electron delocalization of electrons within the π aromatic system (Figure S7). Detailed Raman and IR studies before and after sulfurization also showed the integrity of the –C=N functionalities of the benzimidazole linkage between 1615–1635 cm^{-1} (Figure 2C, Figure S8). However, the intensity of the signal for –C–F bonds in DUT-178, observed only in Raman at 695 cm^{-1} was diminished with the appearance of new signals for C–S bond formation at 927 cm^{-1} and 1006 cm^{-1},[37] as well as signals from covalently anchored sulfur chains (S_3–S_5) at 544 cm^{-1}[38] in S-DUT-178 (Figure 2C). IR shows intensified and combined peak broadening for the benzimidazole –NH and polysulfide terminal –SH in the range of 2500 cm^{-1} to 3400 cm^{-1} (Figure S8).[39]

Activation of the sulfurized polymer at 100 °C under vacuum helps to remove the unbound or elemental sulfur present in the polymer, as confirmed by the absence of diffraction peaks belonging to elemental sulfur in PXRD (Figure S9) and any low-frequency < 400 cm^{-1} sulfur signal in the Raman studies (Figure 2C). The covalent anchoring of sulfur results in a 30–32 wt% loading of sulfur, calculated taking into account the decomposition temperature of the as-made polymer at 400 °C and the decomposition temperature of the sulfurized polymer at 340 °C, as observed in TGA-DTA measurements (Figure 2D). TGA analysis coupled with a mass spectrometer confirmed two steps of thermal decomposition of these strongly covalent anchored polysulfides at a high temperature of 400 °C by the emission of sulfur monoxide (SO) or sulfur dioxide (SO_2) gases (Figure S10).

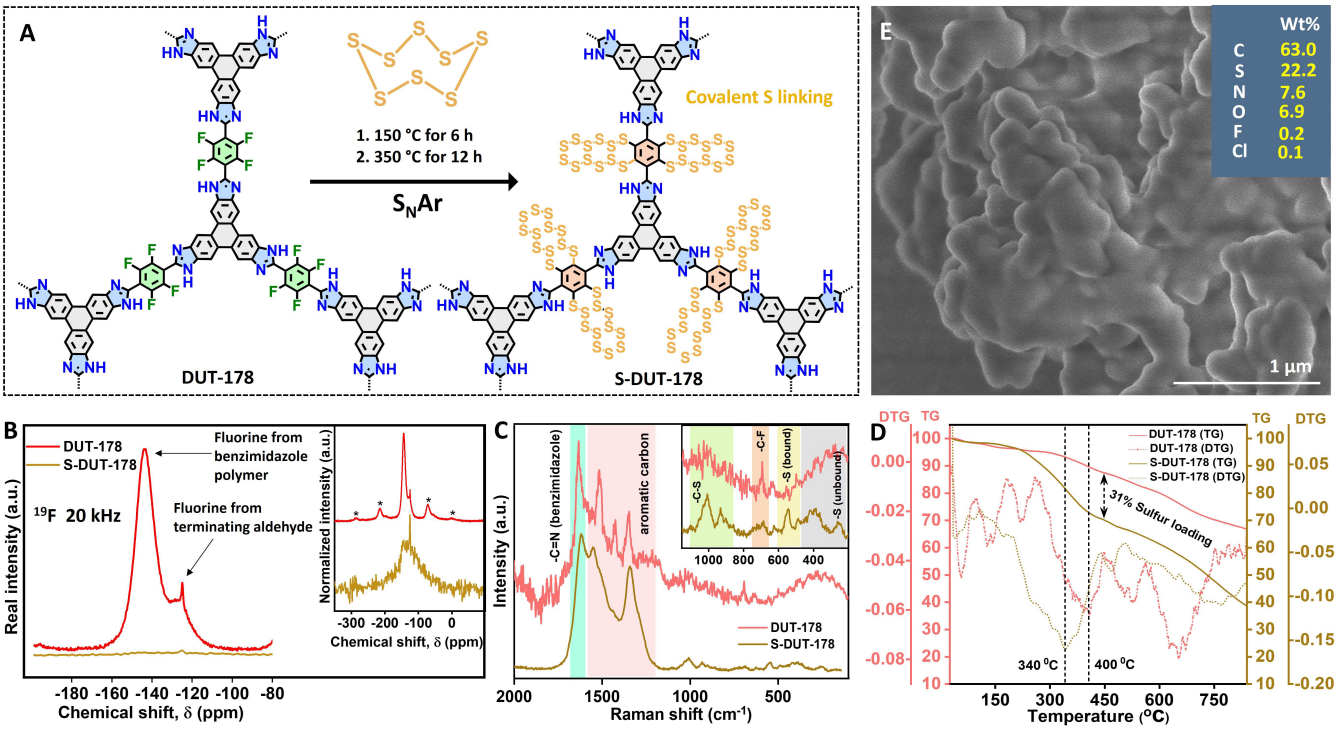

Figure 2. A. Sulfurization of DUT-178 for covalent anchoring of the polysulfide in S-DUT-178. **B**. The real intensity comparison of ^{19}F depth MAS NMR spectra of DUT-178 with S-DUT-178. A zoomed version showing nearly 35 times the normalized intensity spectra of these two materials. **C**. Raman shifts the DUT-178 with S-DUT-178 showing the integrity of benzimidazole linkage. The inset showed the appearance of signals from the –C–S and covalently bound sulfur chains. **D**. TGA-DTA plots of the DUT-178 and S-DUT-178 indicated more than 30% mass loss from the S-DUT-178 for anchored polysulfide. **E**. FE-SEM images of the S-DUT-178 showed the integrity of the amalgamated flakes of the polymer. Inset showing the elemental analysis from EDX.

However, the inherent porosity of the polymer was significantly lost due to the occupancy of covalently anchored polysulfide chains (Figure S11). Interestingly, the planarity of the triphenylene building units and the chemically robust aromatic benzimidazole linkage assisted in maintaining the flake-like morphology of the S-DUT-178 polymer

(Figure 2E, Figure S12). Energy-dispersive X-ray analysis (EDX) and elemental mapping show a homogeneous distribution of sulfur throughout the organic skeleton of the polymer and a drastic drop in the overall fluorine content due to sulfur enrichment (Figure S13).

Lithium-sulfur battery studies with S-DUT-178 derived coin-cells

This electronically conjugated benzimidazole-linked polymer is covalently anchored with polysulfide chains, and it showed great potential to overcome the polysulfide dissolution problem in standard sulfur batteries. To investigate its advantages, a convenient and easily configurable Li–S battery was constructed. A slurry of N-Methyl-2-pyrrolidone (NMP) solution containing 70% S-DUT-178, 20% Super P carbon, and 10% polyvinylidene fluoride (PVDF) binder composite was coated on an aluminum current collector as a working electrode. This was combined with a Li-metal counter electrode, in the presence of an ether-based electrolyte system i.e. 1 M lithium bis-(trifluoromethanesulfonyl) imide (LiTFSI) in dioxolane (DOL): dimethoxyethane (DME) (1:1) with 0.1 M lithium nitrate ($LiNO_3$) for operating a Li–S battery within the 1.8 to 2.6 V potential window. The configured cell exhibited reasonable electrode-electrolyte charge transfer resistance in the Nyquist plot of electrochemical impedance spectroscopy data at open circuit potential (OCP) while measuring at a high-frequency region (Figure S14). This particularly highlights the importance of a good conjugated pathway in the sulfurized polymer cathode. The lower slope of the 'Warburg' tail of the impedance plot at the low-frequency region indicated a high diffusivity of the electrolyte ions through a moderately porous backbone. These properties enable the electrochemical activity of the covalently anchored polysulfides, as observed in the cyclic voltammogram (CV) of the derived coin cell. The voltammogram showed a low-intensity peak at 2.3 V (Figure 3A(i)), corresponding to the lithiation of long-chain polysulfide scaffolds, and a high-intensity peak at 2.1 V for the lithiation of the short-length polysulfide chains,[40] exhibiting great reversibility during reverse bias at 2.37 V across consecutive cycles. In contrast, the current density for the sulfur lithiation and delithiation gradually decreases with the progression of the cycles when porous Ketjen black is just impregnated with elemental sulfur without having any covalent connection (Figure S15A). Increasing the sweep rate elevated the difference of lithiation and delithiation potential of S-DUT-178, achieving moderate kinetics for redox activity from the sulfur entities even in faster interaction times of lithium (Figure 3 A(ii)). This is superior compared to elemental S@ketjenblack which typically fails at high scan rates due to a lack of electron flow to the sulfur entities (Figure S15B). At an applied current density of 100 mA/g, the first discharge plateau, observed near 2.3 V in the initial galvanostatic charge-discharge (GCD) plot (as shown in Figure 3B(i)), suggests a partial dissolution of Li-polysulfides from long-chain anchored polysulfides. This degradation may occur from the open end of

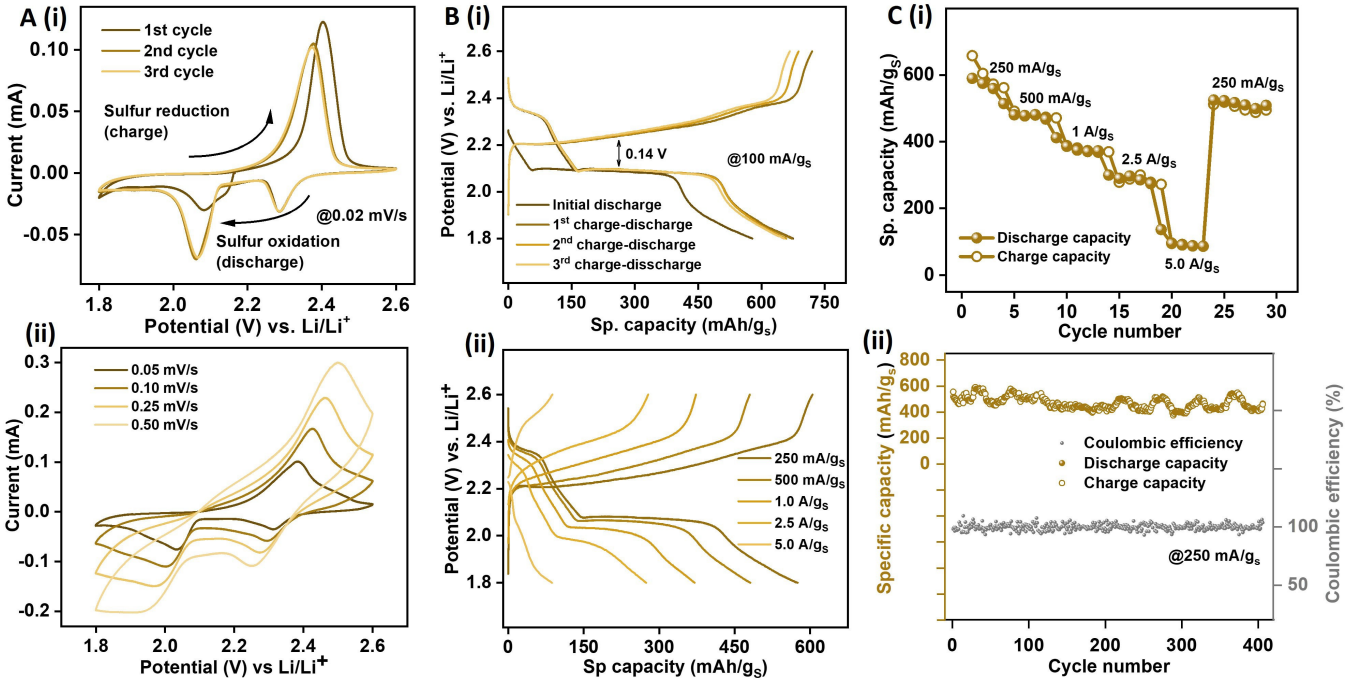

Figure 3. A. Cyclic voltammogram of S-DUT-178-derived coin cell of Li–S battery at (**i**). 0.2 mV/s scan rates for the initial 3 cycles, and (**ii**). elevated different scan rates. **B**. Charge–discharge profiles of the S-DUT-178-derived coin cell at (**i**). 100 mA/g_s, and at (**ii**) other current densities. **C**. (**i**). Rate performance of the S-DUT-178-derived coin cell at different current densities. (**ii**). Cycle stability of the S-DUT-178-derived coin cell at a current density of 250 mA/g.

the polysulfides that are not covalently connected to the polymer skeleton.[39] However, the confinement effect of this Li-polysulfide species helped to trap it near the framework for reversible covalent connectivities. The second long discharge plateau, from 2.1 to 2.07 V, induced the formation of many Li-polysulfide species which are expected to be covalently bound to the polymer.[40] This Li-polysulfide species needs to be reversibly transformed to the initial polysulfide chains to ensure the cyclability of the electrode. The charge-discharge with increasing current densities showed a loss of specific capacity due to slower diffusion kinetics of the mobile ions (Figure 3 C(i)). However, it still retained 52% of the overall specific capacities, going from 250 mA/g to 2.5 A/g, which is quite a good improvement compared to S@ketjenblack (Figure S15C and S15D). The reason for this improvement is the lower overpotential of S-DUT-178 derived coin-cells even at higher current densities while going beyond 250 mA/g_S, the overpotential increases drastically for the S@ketjenblack (Figure S15B). Sulfur-immobilized frameworks have a high sulfur percentage and high initial specific capacity due to physisorption or chemisorption, but lack of covalent linkage, making them unsuitable for fast charging (Scheme S4).[41,42,43] Covalently anchored polysulfides offer through-bond electronic communication, allowing for faster charging and better capacity retention at higher current densities, despite lower sulfur loading. The strong covalent anchoring of polysulfides in S-DUT-178 results in a lower polysulfide shuttle, leading to greater cycling stability. This stability was observed through a considerably low loss of specific capacity of only 16% over 400 cycles of charge-discharge, which amounts to 0.04% per cycle at 250 mA/g_s (Figure 3C(ii)). The comparison table of Li–S battery performance (Table S1), using covalently anchored polysulfides containing electrodes derived from amorphous and crystalline materials, clearly shows that amorphous polymer-derived materials exhibit better retention of specific capacity over cycles compared to crystalline covalent organic framework (COF)-derived materials. Post-cycling analysis, following surface treatment, revealed intact Raman signals from the anchored polysulfides (–S–S: 476 cm^{-1}, 544 cm^{-1} and –C–S: 927 cm^{-1}, 1006 cm^{-1}) and the benzimidazole linkage (–C=N: 1611 cm^{-1}) (Figure S16). This indicated the chemical and electrochemical stability of the electrodes, even after multiple cycles, attributed to the robust and aromatic benzimidazole linkage in the framework, safeguarding against degradation under applied potential.

Aluminum-sulfur battery studies with S-DUT-178 derived Swagelok-cell

Furthermore, the applicability of S-DUT-178 as an advanced working electrode was explored in a more cost-effective sulfur battery, specifically Al–S batteries,[44] where abundant aluminum metal served as the counter electrode and offered multi-electron transfer capability. To derive this, 65% S-DUT-178 was mixed with a 25% conductive Super P carbon additive and 10% PVDF binder and coated onto a niobium current collector to configure the working electrode. The glassy fiber separator within these two electrodes was then sandwiched by treating with chloroaluminate ionic liquid electrolyte [aluminum chloride ($AlCl_3$) mixed with 1-ethyl-3-methylimidazolium chloride (EMICl) in a 1.3 : 1 molar ratio][45] for constructing a stable and low resistivity Swagelok cell with appreciable charge transfer resistance (Figure S17).

The mechanism of this battery does not follow the typical metal-sulfur batteries with simple Al^{3+} interactions with sulfur. Instead, the electrolyte containing $Al_2Cl_7^-$ acts as an active agent, leading to the formation of Al_2S_X species during discharging.[44] However, the poor cyclability and reversibility of this low-cost battery are associated with the dissolution of in-situ forming polysulfides in the ionic liquid electrolyte, similar to what is observed in Li–S batteries. Hence, the covalently anchored polysulfide of S-DUT-178 holds great potential for improving its capacity retention. The CV and GCD measurements on this constructed aluminum-sulfur battery reveal a significant concentration polarization at low voltage, ranging from 0.3 V to 0.15 V (Figure 4A, resulting in a high depth of discharge (DoD) of the cell (Figure 4B).[46] This indicates the challenges associated with the very slow mass transfer and ion diffusion from the aluminum electrode surface to the S-DUT-178-derived electrode surface due to the high viscosity and higher ionic resistivity of the electrolyte used. This also narrowed down the overall voltage of the battery from only 0.15 V to 1 V and showed a very high cell overpotential of 0.73 V, rendering this battery impractical.

However, inspired by recent studies by Yang and co-workers, a new electrolyte system [aluminum chloride ($AlCl_3$) mixed with 1-ethyl-3-methylimidazolium bromide (EMIBr) in a 1.3 : 1 molar ratio] was employed,[47] which acted as a source of $Al_2Cl_6Br^-$ active ions for reacting with the covalently anchored sulfur atoms. According to their studies, this $Al_2Cl_6Br^-$ exhibits a lower activation barrier, enabling easy dissociation of Al–Cl bonds to produce discharging species of Al_2S_X. As a result, the overpotential of the oxidation-reduction in the CV plot (Figure 4A) of the configured battery was decreased from 0.73 V to 0.48 V, suppressing the negative effect of the concentration polarization in the charge-discharge curve (Figure 4B). This new electrolyte system comfortably operates the Al–S battery within the voltage window of 0.2 to 1.5 V, achieving 92–95% coulombic efficiency and 460 mAh/g_S specific capacities in each charge-discharge cycle (Figure 4C). The lower coulombic efficiency indicates an irreversible oxidation of sulfur-containing cathode due to the partial decomposition of organic parts of the cathodes. Further optimization may improve this efficiency by employing a proper electrolyte system and increasing the percentage of sulfur in the working electrode. Understanding covalent polysulfide anchoring brings the advantage of stabilizing the specific capacity up to 40% even after 170 charge-discharge cycles at a low current density of 50 mA/g (Figure 4D), something

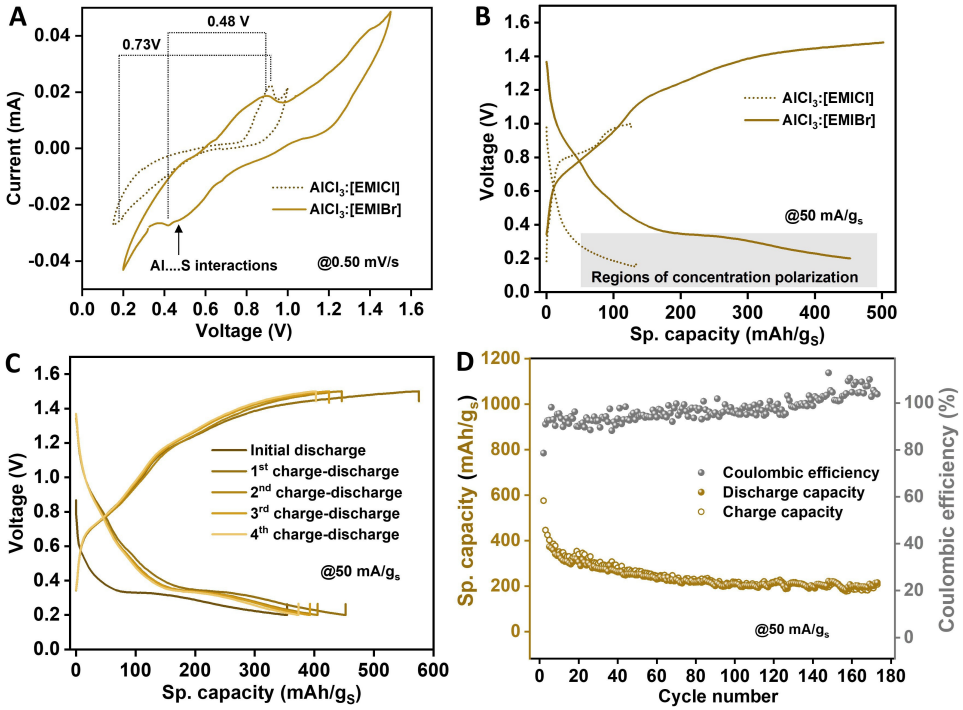

Figure 4. A. Cyclic voltammogram of S-DUT-178-derived Swagelok-cell of Al–S battery at 0.5 mV/s scan rate using two different electrolyte systems consisting of $AlCl_3$-EMICl and $AlCl_3$-EMIBr ionic liquids. **B**. The difference of charge-discharge profiles at 50 mA/g_s current density while treating with $AlCl_3$-EMICl and $AlCl_3$-EMIBr ionic liquid-based electrolytes. **C**. The charge-discharge cycles using best-performing $AlCl_3$-EMIBr ionic liquid-based electrolytes at 50 mA/g_s current density. **D**. Cycle stability of the S-DUT-178-derived Swagelok cell up to 170 cycles at 50 mA/g_s current density.

which is still very difficult to achieve with sulfur-doped carbon materials.

Conclusions

The abundance of p-block elements and their intriguing redox activities offer huge potential for developing energy storage materials cost-effectively. Among these elements, sulfur stands out as an abundant and economical electrode material, holding promise for constructing futuristic high-capacity batteries. However, concerns about their stabilities under potential and dissolution in electrolyte systems have hindered their practical applicability. This study addresses the issue by introducing an easily synthesizable designer polymer that covalently integrates polysulfides, thereby opening the door for a stable battery configuration. By optimizing the loading of sulfur entities in the electrode, the gravimetric capacities can be improved, and using a proper conjugated host may enhance the redox kinetics, resulting in faster charging battery configurations. The applicability of this polymer extends not only to standard Li–S batteries but also to Al–S batteries, where Al, a cheaper and more abundant metal, acts as a counter electrode, constructing a full battery and including electrolytes mostly from p-block elements. To properly understand the complexity of the internal mechanism and redox chemistry in such batteries, it is crucial to employ proper design and molecular engineering of the reticular polymer and introduce operando characterization techniques during the redox steps. The choice of electrode-electrolyte compatibility may present a challenging issue for these new battery systems in optimizing the working potential window. Reducing the mass of the redox-inactive entities in the electrode could aid in achieving higher charge storage ability. In this regard, the reticular growth of the polymer through selective functional group incorporation can pave the way for a proper electrode configuration with enhanced redox activity.

Supporting Information

Experimental procedures, NMR spectra, Raman studies, FTIR spectra, PXRD patterns, nitrogen isotherms, BET plots, TGA data, FE-SEM images, HR-TEM images, electrochemical methods and electrochemical data including CV, GCD, impedance data. Additional references cited within the Supporting Information.[19,39,48,49,50,51,52,53,54,55]

Acknowledgements

This work was supported by the DFG Priority Programme "Polymer-based Batteries" (SPP 2248). We are very much thankful to our co-project investigator of SPP 2248 Prof. Dr. Eike Brunner, Bioanalytical Chemistry, TU Dresden for providing the facilities for conducting NMR studies and for guiding us to analyze the data. The authors are grateful for the support from the collaborative research center "Chemistry of Synthetic 2D Materials" funded by the Deutsche Forschungsgemeinschaft (DFG, German Research Foundation)–SFB-

1415-417590517. A.S. gratefully acknowledges the Fonds der Chemischen Industrie for a Liebig Fellowship. Open Access funding enabled and organized by Projekt DEAL.

Conflict of Interests

The authors declare no conflict of interest.

Data Availability Statement

The data that support the findings of this study are available from the corresponding author upon reasonable request.

Keywords: Fluorinated Polymer · Benzimidazole-linkage · Polysulfide Anchoring · Sulfur batteries

[1] D. Larcher, J.-M. Tarascon, *Nat. Chem.* **2015**, *7*, 19–29.
[2] B. P. Koirala, E. van Oost, H. van der Windt, *Appl. Energy* **2018**, *231*, 570–585.
[3] C. Liu, F. Li, L.-P. Ma, H.-M. Cheng, *Adv. Mater.* **2010**, *22*, E28–62.
[4] P. Murugan, R. D. Nagarajan, B. H. Shetty, M. Govindasamy, A. K. Sundramoorthy, *Nanoscale advances* **2021**, *3*, 6294–6309.
[5] J.-K. Yoo, J. Kim, Y. S. Jung, K. Kang, *Adv. Mater.* **2012**, *24*, 5452–5456.
[6] W. Tang, Y. Liu, C. Peng, M. Y. Hu, X. Deng, M. Lin, J. Z. Hu, K. P. Loh, *J. Am. Chem. Soc.* **2015**, *137*, 2600–2607.
[7] H. Liu, K. Hu, D. Yan, R. Chen, Y. Zou, H. Liu, S. Wang, *Adv. Mater.* **2018**, *30*, e1800295.
[8] L. Ma, J. Wu, Y. Li, Y. Lv, B. Li, Z. Jin, *Energy Storage Mater.* **2021**, *42*, 723–752.
[9] S. Chen, J. Zhang, *Dalton Trans.* **2020**, *49*, 9929–9934.
[10] X. Huang, B. Luo, P. Chen, D. J. Searles, D. Wang, L. Wang, *Coord. Chem. Rev.* **2020**, *422*, 213445.
[11] R. Zou, W. Liu, F. Ran, *InfoMat* **2022**, *4*, e12319.
[12] A. F. Hofmann, D. N. Fronczek, W. G. Bessler, *J. Power Sources* **2014**, *259*, 300–310.
[13] S. Zeng, G. M. Arumugam, X. Liu, Y. Yang, X. Li, H. Zhong, F. Guo, Y. Mai, *Small* **2020**, *16*, e2001027.
[14] Z. Cheng, H. Pan, H. Zhong, Z. Xiao, X. Li, R. Wang, *Adv. Funct. Mater.* **2018**, *28*, 1707597.
[15] J. Zhou, R. Li, X. Fan, Y. Chen, R. Han, W. Li, J. Zheng, B. Wang, X. Li, *Energy Environ. Sci.* **2014**, *7*, 2715.
[16] H. Liao, H. Ding, B. Li, X. Ai, C. Wang, *J. Mater. Chem. A* **2014**, *2*, 8854–8858.
[17] R. Yan, B. Mishra, M. Traxler, J. Roeser, N. Chaoui, B. Kumbhakar, J. Schmidt, S. Li, A. Thomas, P. Pachfule, *Angew. Chem. Int. Ed.* **2023**, *62*, e202302276.
[18] R. Fang, J. Xu, D.-W. Wang, *Energy Environ. Sci.* **2020**, *13*, 432–471.
[19] D.-G. Wang, N. Li, Y. Hu, S. Wan, M. Song, G. Yu, Y. Jin, W. Wei, K. Han, G.-C. Kuang, W. Zhang, *ACS Appl. Mater. Interfaces* **2018**, *10*, 42233–42240.
[20] Y. Xu, S. Jin, H. Xu, A. Nagai, D. Jiang, *Chem. Soc. Rev.* **2013**, *42*, 8012–8031.
[21] J. F. Bunnett, *Q. Rev. Chem. Soc.* **1958**, *12*, 1.
[22] S. H. Je, H. J. Kim, J. Kim, J. W. Choi, A. Coskun, *Adv. Funct. Mater.* **2017**, *27*, 1703947.
[23] M. G. Rabbani, H. M. El-Kaderi, *Chem. Mater.* **2011**, *23*, 1650–1653.
[24] M. G. Rabbani, H. M. El-Kaderi, *Chem. Mater.* **2012**, *24*, 1511–1517.
[25] X. Yu, A. Manthiram, *Adv. Energy Mater.* **2017**, *7*, 1700561.
[26] S.-H. Chung, A. Manthiram, *Adv. Mater.* **2019**, *31*, e1901125.
[27] C. H. Roeder, A. R. Day, *J. Org. Chem.* **1941**, *06*, 25–35.
[28] L. Chen, J. Kim, T. Ishizuka, Y. Honsho, A. Saeki, S. Seki, H. Ihee, D. Jiang, *J. Am. Chem. Soc.* **2009**, *131*, 7287–7292.
[29] P. Das, S. K. Mandal, *Chem. Mater.* **2019**, *31*, 1584–1596.
[30] S. Nandi, S. K. Singh, D. Mullangi, R. Illathvalappil, L. George, C. P. Vinod, S. Kurungot, R. Vaidhyanathan, *Adv. Energy Mater.* **2016**, *6*, 1601189.
[31] Z. Tošner, R. Andersen, B. Stevensson, M. Edén, N. C. Nielsen, T. Vosegaard, *J. Magn. Reson.* **2014**, *246*, 79–93.
[32] A. H. Khan, B. Barth, M. Hartmann, J. Haase, M. Bertmer, *J. Phys. Chem. C.* **2018**, *122*, 12723–12730.
[33] A. Kubo, T. P. Spaniol, T. Terao, *J. Magn. Reson.* **1998**, *133*, 330–340.
[34] M. Robin Bendall, R. E. Gordon, *J. Magn. Reson. (1969-1992)* **1983**, *53*, 365–385.
[35] S. A. Reinsberg, S. Ando, R. K. Harris, *Polymer* **2000**, *41*, 3729–3736.
[36] I. M. El-Nahhal, J. J. Yang, I.-S. Chuang, G. E. Maciel, *J. Non-Cryst. Solids* **1996**, *208*, 105–118.
[37] P. Bazylewski, R. Divigalpitiya, G. Fanchini, *RSC Adv.* **2017**, *7*, 2964–2970.
[38] B. P. Vinayan, T. Diemant, X.-M. Lin, M. A. Cambaz, U. Golla-Schindler, U. Kaiser, R. Jürgen Behm, M. Fichtner, *Adv. Mater. Interfaces* **2016**, *3*, 1600372.
[39] S. Haldar, M. Wang, P. Bhauriyal, A. Hazra, A. H. Khan, V. Bon, M. A. Isaacs, A. De, L. Shupletsov, T. Boenke, J. Grothe, T. Heine, E. Brunner, X. Feng, R. Dong, A. Schneemann, S. Kaskel, *J. Am. Chem. Soc.* **2022**, *144*, 9101–9112.
[40] C. Barchasz, F. Molton, C. Duboc, J.-C. Leprêtre, S. Patoux, F. Alloin, *Anal. Chem.* **2012**, *84*, 3973–3980.
[41] Y. Zhu, J. Yang, X. Qiu, M. Li, G. He, Q. Wang, Z. Xie, X. Li, H. Yu, *ACS Appl. Mater. Interfaces* **2021**, *13*, 60373–60383.
[42] B.-Y. Lu, Z.-Q. Wang, F.-Z. Cui, J.-Y. Li, X.-H. Han, Q.-Y. Qi, D.-L. Ma, G.-F. Jiang, X.-X. Zeng, X. Zhao, *ACS Appl. Mater. Interfaces* **2020**, *12*, 34990–34998.
[43] Z. Li, H.-Y. Zhou, F.-L. Zhao, T.-X. Wang, X. Ding, B.-H. Han, W. Feng, *Chin. J. Polym. Sci.* **2020**, *38*, 550–557.
[44] M. Klimpel, M. V. Kovalenko, K. V. Kravchyk, *Communications chemistry* **2022**, *5*, 77.
[45] W. A. Appiah, H. Li, J. Lampkin, J. M. García-Lastra, *J. Power Sources* **2022**, *529*, 231254.
[46] J. Kim, J. Kowal, *Batteries* **2021**, *7*, 76.
[47] H. Yang, L. Yin, J. Liang, Z. Sun, Y. Wang, H. Li, K. He, L. Ma, Z. Peng, S. Qiu, C. Sun, H.-M. Cheng, F. Li, *Angew. Chem. Int. Ed.* **2018**, *57*, 1898–1902.
[48] S. Haldar, P. Bhauriyal, A. R. Ramuglia, A. H. Khan, S. de Kock, A. Hazra, V. Bon, D. L. Pastoetter, S. Kirchhoff, L. Shupletsov, A. De, M. A. Isaacs, X. Feng, M. Walter, E. Brunner, I. M. Weidinger, T. Heine, A. Schneemann, S. Kaskel, *Adv. Mater.* **2023**, *35*, e2210151.
[49] Q. Jiang, Y. Li, X. Zhao, P. Xiong, X. Yu, Y. Xu, L. Chen, *J. Mater. Chem. A* **2018**, *6*, 17977–17981.
[50] J.-M. Chen, H. Duan, Y. Kong, B. Tian, G.-H. Ning, D. Li, *Energy Fuels* **2022**, *36*, 5998–6004.
[51] F. Xu, S. Yang, G. Jiang, Q. Ye, B. Wei, H. Wang, *ACS Appl. Mater. Interfaces* **2017**, *9*, 37731–37738.
[52] W. J. Chung, J. J. Griebel, E. T. Kim, H. Yoon, A. G. Simmonds, H. J. Ji, P. T. Dirlam, R. S. Glass, J. J. Wie, N. A. Nguyen, B. W. Guralnick, J. Park, A. Somogyi, P. Theato, M. E. Mackay, Y.-E. Sung, K. Char, J. Pyun, *Nat. Chem.* **2013**, *5*, 518–524.
[53] J. Yan, B. Li, X. Liu, *Nano Energy* **2015**, *18*, 245–252.
[54] A. Bhargav, M. E. Bell, Y. Cui, Y. Fu, *ACS Appl. Energ. Mater.* **2018**, *1*, 5859–5864.
[55] H. Hu, B. Zhao, H. Cheng, S. Dai, N. Kane, Y. Yu, M. Liu, *Nano Energy* **2019**, *57*, 635–643.

Manuscript received: August 24, 2023
Accepted manuscript online: October 25, 2023
Version of record online: November 13, 2023